Seismic velocity structure of the slab and continental plate in the region of the 1960 Valdivia (Chile) slip maximum — Insights into fluid release and plate coupling

Yvonne Dzierma [a,*], Wolfgang Rabbel [a], Martin Thorwart [a], Ivan Koulakov [b], Heidi Wehrmann [c], Kaj Hoernle [c], Diana Comte [d]

[a] SFB 574 and Christian-Albrechts University Kiel, Inst. Geosciences, Dep. Geophysics, Otto-Hahn-Platz 1, D-24118 Kiel, Germany
[b] Institute for Petroleum Geology and Geophysics, SB RAS, Prospekt Akademika Koptuga, 3, Novosibirsk 630090, Russia
[c] SFB 574 and GEOMAR, Wischhofstr. 1–3, 24148 Kiel, Germany
[d] Universidad de Chile, AMTC-Departamento de Geofísica, Blanco Encalada 2002, Casilla 2777, Santiago, Chile

ARTICLE INFO

ABSTRACT

The south-central Chilean subduction zone has witnessed some of the largest earthquakes in history, making this region particularly important for understanding plate coupling. Here we present the results of a local earthquake tomography study from a temporary local seismic network in the Villarrica region between 39 and 40°S, where the largest coseismic displacement of the 1960 Valdivia earthquake occurred. A low-velocity anomaly and high Vp/Vs values occur under the coastal region, indicating mantle serpentinisation and/or underthrusting of forearc material. Further east, a high-velocity anomaly is observed, interpreted as "normal" high-velocity mantle. Under the active volcanic arc a low-velocity anomaly together with high Vp/Vs ratios (1.8 and higher) likely images fluid ascent beneath the volcanoes. Close to the subducting Valdivia Fracture Zone, the coastal low-velocity anomaly extends further inland, where it interrupts and shifts the high-velocity anomalies associated with "normal" fast mantle velocities. This may indicate enhanced fluid presence along this part of the margin, probably caused by a stronger hydration of the incoming plate along the Valdivia Fracture Zone. This is consistent with geochemical fluid proxies (U/Th, Pb/Ce, Ba/Nb) in young volcanic rocks displaying peak values along the volcanic front at Llaima and Villarrica Volcanoes, and with recent GPS measurements, which suggested a local reduction in plate coupling in this region. The shift in the high-velocity anomaly underlying the central part may be caused by a north to south decrease in plate age and hydration across the Valdivia Fracture Zone, and may explain why a Central Valley is absent in this segment of the margin. The low La/Yb ratios in the volcanic rocks from Villarrica and Llaima suggest that the high slab-derived fluid flux causes elevated degrees of melting beneath these volcanoes, providing an explanation as to why these are amongst the most active volcanoes in South America.

1. Introduction

Characterising the properties of subduction zones susceptible to great earthquakes and tsunamis is a major challenge for the Earth sciences. Over the past years, it has been established that the presence of fluids at the plate boundary is a first-order process determining the position and extent of the seismogenic zone (Hyndman et al., 1997; Ranero et al., 2008). In this model, the plate interface down to depths corresponding to 100–150 °C is well lubricated by fluids released from sediment dehydration reactions; below these depths, the amount of fluids declines and seismic coupling is increased, leading to the onset of seismogenic behaviour. Along the trench, lateral variations in the potential for generating large interseismic strain

accumulation (and hence high seismic moment release) are determined to a large degree by variations in the strength of interplate coupling. In addition to fluid effects along the plate interface and in the mantle wedge, this depends on a variety of properties of the overriding and downgoing plate (age of the slab, subduction velocity and slab dip, plate thickness, roughness and bathymetric features) and sediment present in the trench and along the plate interface. After initiation of an earthquake, the rupture propagation can also be influenced by the presence or absence of bathymetric highs such as ridges and seamounts on the subducting slab, which have been observed to stall earthquake rupture (Robinson et al., 2006; Sparkes et al., 2010).

Globally, megathrust earthquakes are observed to repeatedly recur along the same margin segments (but not necessarily equivalent in magnitude and/or in rupture areas), which appear to be particularly prone to large seismic moment release (Beck et al., 1998; Comte et al., 1986). Some of the largest recorded earthquakes

* Corresponding author. Tel.: +49 431 880 2785; fax: +49 431 880 4432.
E-mail address: ydzierma@geophysik.uni-kiel.de (Y. Dzierma).

on Earth have occurred along the Chilean margin (e.g., Barrientos, 2007; Lomnitz, 2004; Moernaut et al., 2007), making this region particularly important for understanding the mechanisms and consequences of plate coupling in subduction zones. The largest instrumentally recorded earthquake, the Mw = 9.5 1960 Valdivia earthquake, occurred along the south-central Chilean subduction zone and ruptured more than 1000 km length of the plate margin (Barrientos and Ward, 1990; Moreno et al., 2009). The northern part of this region was again recently ruptured during the 2010 Mw = 8.8 Maule earthquake (Delouis et al., 2010; Moreno et al., 2010). Along with strong earthquakes, this region exhibits some of the most active volcanoes of South America, Villarrica and Llaima (Dzierma and Wehrmann, 2010; Stern, 2004). The particularly strong tectonic activity of this location of the Chilean subduction zone likely indicates a special character of the processes of the coupling zone, which might in turn be related to structural properties of the downgoing slab.

In this work, we focus our seismic studies on the Villarrica region between 39 and 40°S, which is where the largest coseismic displacement of the 1960 Valdivia earthquake occurred (Barrientos and Ward, 1990). Previous studies have expressed contrary opinions with respect to plate coupling along this part of the Chilean margin. While gravimetric results (Alasonati Tašárova, 2007; Hackney et al., 2006) have suggested that coupling is particularly strong between 39° and 40°S due to an anomalous gravity signal observed in this segment of the margin, recent GPS measurements (Moreno et al., 2011) observe a local minimum in coupling between 39 and 40°S, interpreted as aseismic slip. To resolve these contrasting views, we believe it is vital to investigate this part of the margin by analysing the physical structure in terms of P- and S-wave velocities (Vp, Vs) and Vp/Vs velocity ratios. To this effect, we present a local earthquake tomography study based on a temporary local seismic network to image the seismic velocity structure down to 70 km depth, from the Chilean coast into the back-arc in Argentina. Finally we also present geochemical data from mafic to intermediate rocks erupted along the volcanic front in the Southern Volcanic Zone (SVZ), in order to compare the fluid flux beneath the volcanic front in the study area (39–40°S) with other parts of the SVZ (35–43°S).

2. Tectonic setting

In the study region (Fig. 1), the Nazca Plate subducts beneath the South American Plate with a convergence velocity of 73.7 mm/yr (DeMets et al., 2010). The oblique incidence at the NNE-trending Chile Trench has created a 1100 km long trench-parallel slip system running through the Andean chain, the Liquiñe-Ofqui Fault Zone (LOFZ, Cembrano et al., 2000; Rosenau et al., 2006).

The subducting slab is cut by several transform faults, the most prominent of which is the Valdivia Fracture Zone (VFZ) impinging on the trench at 40°S. The VFZ constitutes the boundary between ~26 Ma oceanic crust produced at the East Pacific Rise and younger (18–20 Ma) crust produced at the Chile Rise in the south (Tebbens et al., 1997). Between 70 and 100 km depth, the VFZ is observed to be seismically active, which we interpret as indications for fluid release (Dzierma et al., submitted for publication).

The overriding plate along the South-Central Chilean margin is segmented into three main morphotectonic units (from west to east): the coastal Cordillera, Central Valley, and Main Cordillera, where the active volcanic arc is located (Charrier et al., 2007). From surface geology observations, the Central Valley seems to be absent in the Villarrica region between 39° and 40°S. In addition to the atypical surface geology (Rehak et al., 2008), the Villarrica region is furthermore found to exhibit an unusual negative gravity anomaly of 0 to −50 mGal (Alasonati Tašárova, 2007; Hackney et al., 2006), which contrasts with the positive anomalies found to either side of this region and along the rest of the margin. The boundaries of this anomalous segment coincide with the Mocha-Villarrica Fault Zone (MVFZ) in the north and along a number of smaller faults trending towards the Puyehue-Cordón Caulle Volcano Complex in the south. These WNW-trending fault zones, together with the NS-trending
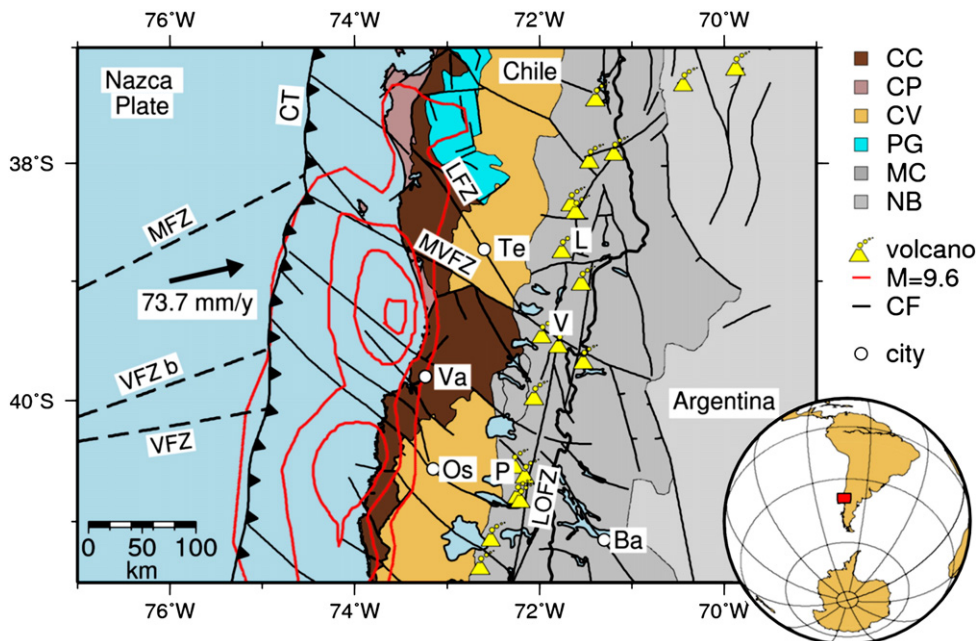

Fig. 1. Tectonic overview. Geologic units: CC — Coastal Cordillera, CP — Coastal Platform, CV — Central Valley, PG — Paleozoic Granites, MC — Main Cordillera and NB — Neuquén Basin. Red contour lines indicate the slip distribution of the 1960 M = 9.6 earthquake for 5 m, 15 m, 25 m and 35 m (Barrientos and Ward, 1990). Black lines show crustal faults (CF) (Melnick and Echtler, 2006). Major faults: LOFZ — Liquiñe-Ofqui-fault zone, MVFZ — Mocha-Villarrica-fault zone, LFZ — Lanalhue fault zone, MFZ — Mocha fracture zone, VFZ — main trace of the Valdivia fracture zone and VFZ b — northern branch of the Valdivia fracture zone. Main volcanoes: V — Villarrica, L — Llaima, P — Puyehue-Cordón Caulle. Major cities shown: Te — Temuco, Va — Valdivia, Os — Osorno and Ba — Bariloche. The black arrow indicates the convergence rate of 73.7 mm/yr and direction of the Nazca Plate relative to the South American Plate. (For interpretation of the references to colour in this figure legend, the reader is referred to the web version of this article.)

Liquiñe-Ofqui Fault Zone, are major determinants for the position of the active volcanic centres (Cembrano and Lara, 2009).

The area to the north (37°–39°S) was recently studied by Bohm (2004) and Haberland et al. (2009) using local earthquake tomography. They found a correlation of the location of the longitudinally oriented Central Valley with high-velocity anomaly in the lower crust and upper mantle. The Coastal Cordillera as well as volcanic arc appeared to be associated with low-velocity anomalies. South of 42°S, Lange (2008) observed similar features. However, the region between these studies has not been seismologically imaged, even though this appears to be the key region for understanding the singular characteristics of this subduction environment. Although broad similarities are observed, the "gap" region is found to be very different from the adjacent areas in geomorphology and gravity (Alasonati Tašárova, 2007; Hackney et al., 2006; Rehak et al., 2008), and has been speculated to present a different stress regime. The processes dominating this environment can only be investigated by establishing the link between these two regions, which is done in the present study.

3. Data set and methods

A temporary seismic network consisting of 15 brand-band stations (Guralp 3ESP-60s) and 40 short-period stations (Mark L-4 C-3D) was operated from December 2008 to November 2009 (Fig. 2, Supplementary Table ST1). All instruments were equipped with EarthDataLoggers.

In addition to the temporary network, we include data for 11 picked events from the University of Chile Seismological Service (SSN) network stations to extend the coverage of our network. Automatic event detection in the continuous data was carried out using a LTA/STA trigger algorithm followed by a network trigger. P- and S-wave onsets were manually picked in the SEISAN software package and located using the optimum 1D velocity model by Bohm et al. (2002). The P phase was picked on the vertical component, the S phase on the horizontal components.

A total of 867 regional events were recorded with epicentral distances less than 500 km, of which 630 events have a location error less than 20 km (both horizontal and vertical) and an rms-

value ≤ 1 s. To estimate the optimal reference velocity distribution, we determined the preliminary locations of the sources using ten 1D velocity models and selected one that provided the minimum value of the average residual (Table 1). The tomographic inversion was performed using the LOTOS code (Koulakov, 2009), which uses the observed P- and S-wave travel times (picks) to invert simultaneously for a 3D image of the P- and S-wave velocities, hypocentres, and station corrections. LOTOS offers two options, inverting either for the P- and S-wave velocities or for the P-wave velocities and V_p/V_s velocity ratio. The presented results were obtained with the first option except for the presented V_p/V_s velocity ratios, which were inverted using the second option which relies on the differential travel times.

Velocity anomalies were computed in nodes distributed inside the study volume according to the ray density. The lateral grid spacing was 5 km; with depth, the spacing was dependent on ray sampling, but was not less than 5 km. The processing consisted of five iterations, of which each contained a source location in the 3D velocity model, matrix calculation and inversion. The inversion was performed simultaneously for the P and S velocities, source corrections (hypocentre coordinates and origin time for each source) and station corrections. The inversion showed convergence after five iterations. We use a level of smoothing of 1.3 for P and 2.2 for S waves. For the 3D inversion we used a total of 5781 P- and 3824 S-phases. The final residuals after five iterations are 0.132 s for P and 0.166 s for S waves, corresponding to a reduction of 35% and 41% in standard deviation, respectively.

4. Ray coverage and resolution

Good ray coverage is generally found at depths between 10 and 40 km, and restricted to smaller areas at greater depth (Fig. 3). In our presentation of the results, we apply a mask based on ray-coverage to mark those regions that suffer from poorer coverage. As all events below 40 km depth occur in or near the subducting slab, we have only few crossing rays to determine the velocity structure at sub-Moho depths. While it is still possible to determine slow- or fast-anomalies from the arrival times, these tend to be smeared
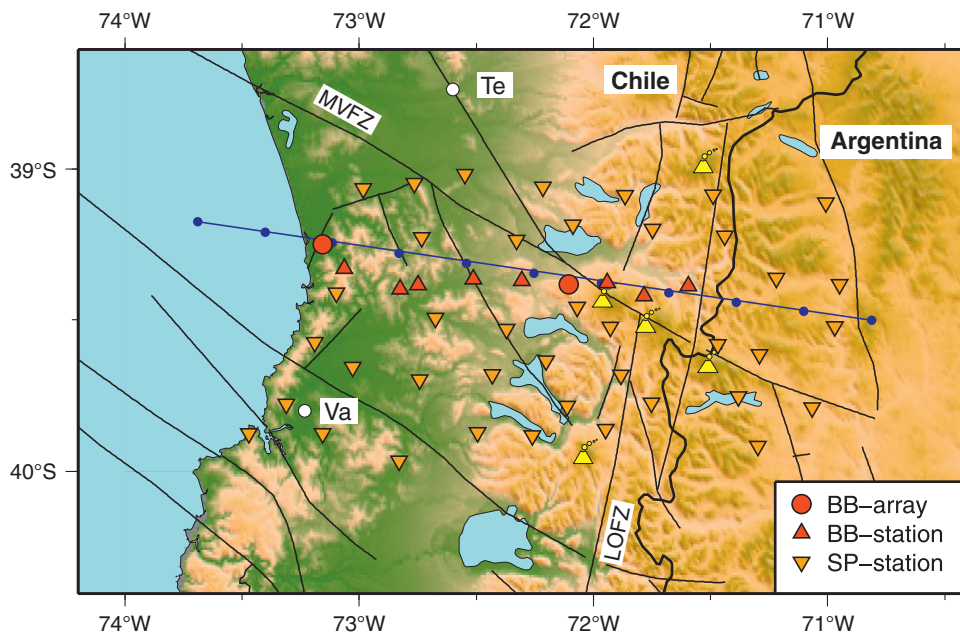

Fig. 2. Local seismic network. Seismic installations: BB-Ar — Array of broadband stations, BB-St — single broadband stations and SP-St — single short period stations. Faults, volcanoes and towns are the same as in Fig. 1. The dotted blue line indicates the position of the vertical profile, with dots placed every 25 km. (For interpretation of the references to colour in this figure legend, the reader is referred to the web version of this article.)

Table 1
1D velocity model used as a starting model in the tomographic inversion.

Depth (km)	Vp (km/s)	Vs (km/s)
−3.0	5.0	2.8
30.0	6.7	3.8
50.0	7.8	4.4
130.0	8.0	4.5
240.0	8.2	4.6
600.0	9	5.1

along the ray paths, so depth recovery is poor in the mantle and close to the Argentinean border.

The resolution capacity of the inversion was tested by several chequerboard tests (Fig. 4, Supplementary Fig. S1). Anomalies as large as 20 km can be resolved nearly perfectly at depths down to 50 km. Smaller-scale anomalies are not well resolved except at shallow depths (Vs anomalies of 10 km scale can be resolved only in the centre of the network, down to 30 km depth). The vertical chequerboards show the above-mentioned smearing effect and only retrieve the integrated velocity effect along the ray path outside the centre of the network.

5. Results

The main result of this study is the 3D distribution of the Vp and Vs anomalies, several slices of which are presented in Fig. 5. A large number of tests were performed to assess the reliability and
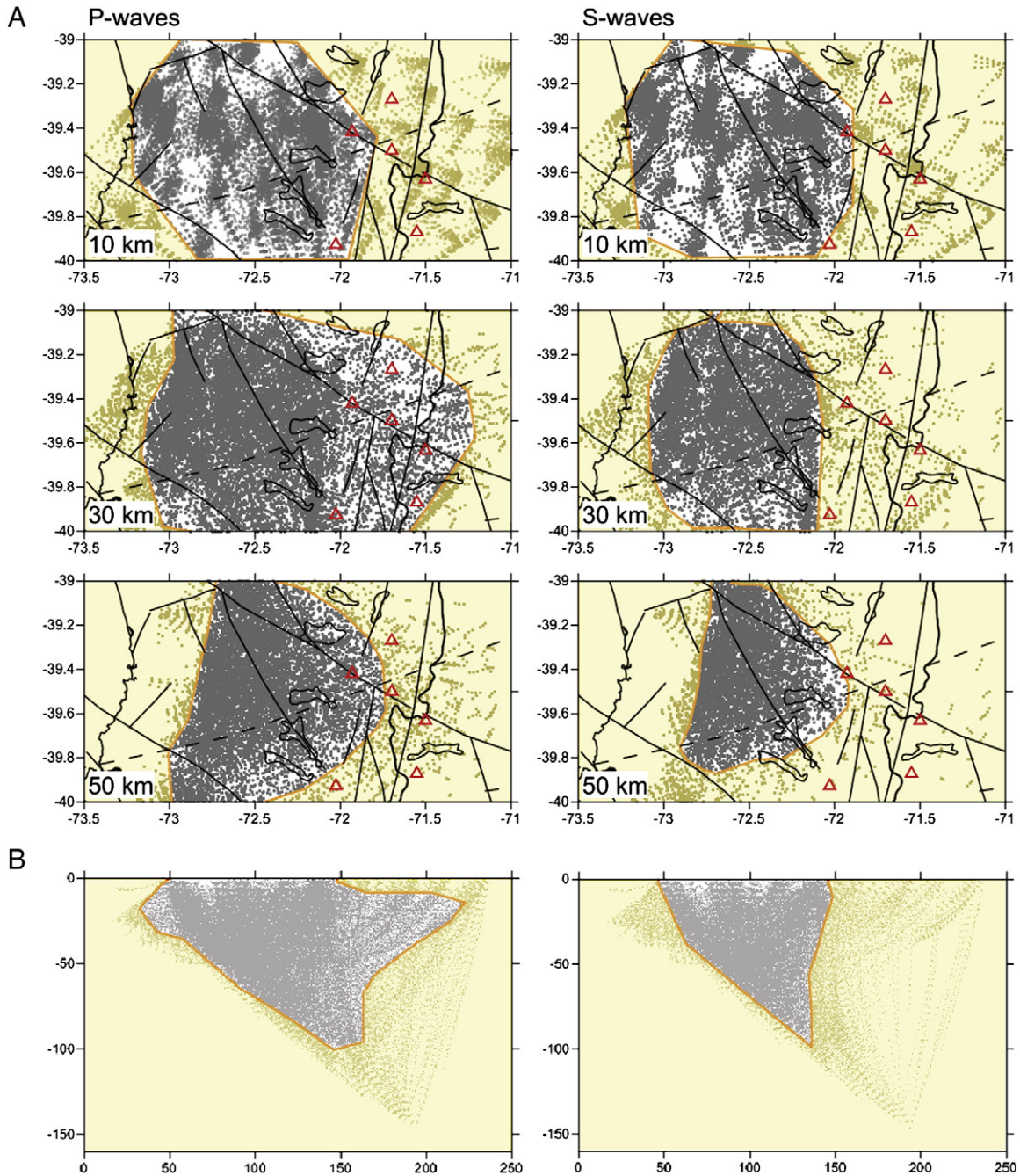

Fig. 3. Ray coverage. A) Rays crossing the 10, 30 and 50 km horizontal planes are displayed as black dots to visualise the ray coverage in the depth sections. Left: Vp, right: Vs. B) Ray coverage of the vertical profile (blue line in Fig. 2).
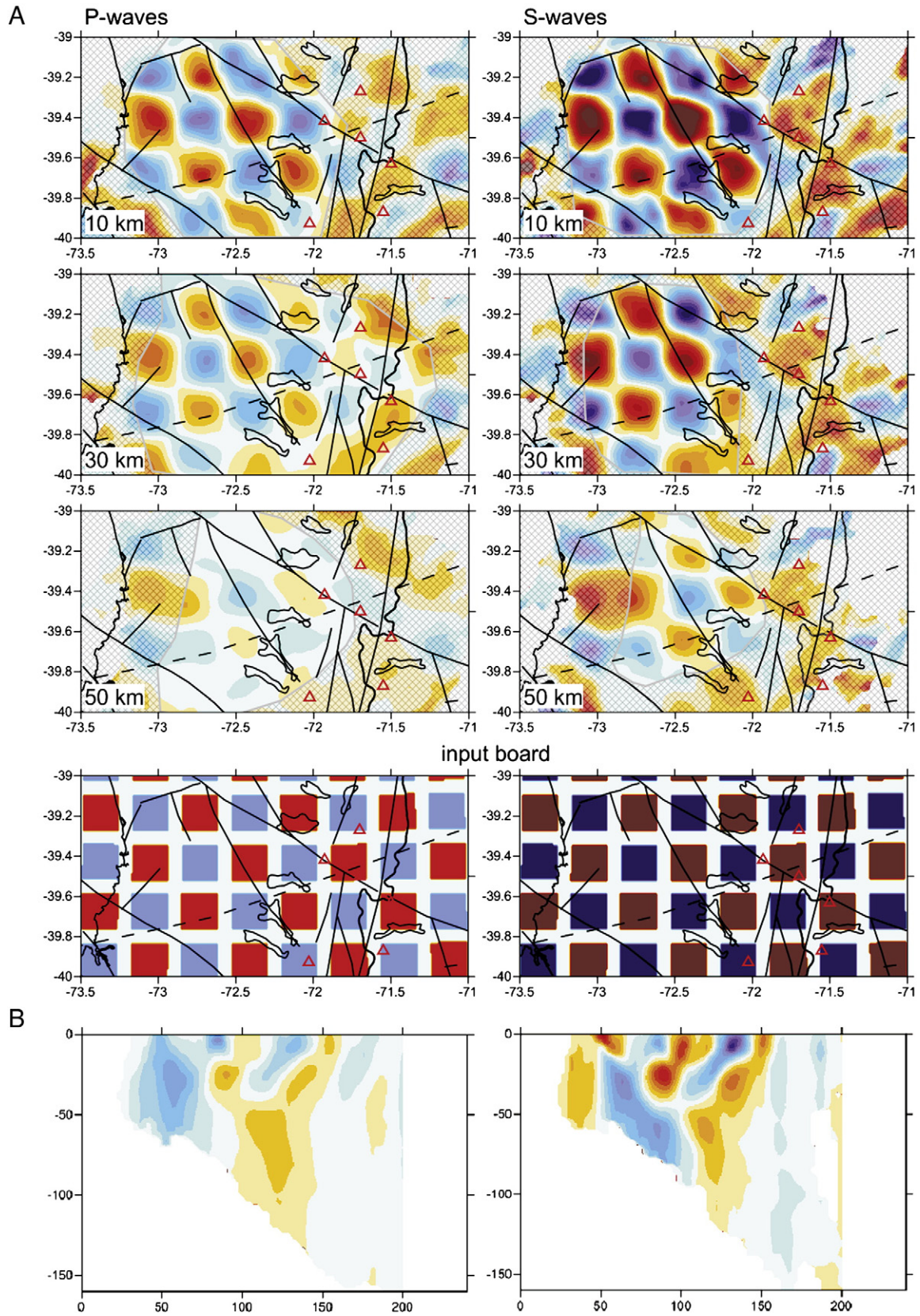
Fig. 4. Chequerboard tests. Chequerboards were calculated for 4% Vp and 7% Vs anomaly, with different board sizes: A) a 20 km wide horizontal board with 7.5 km gap between Vp and Vs anomalies, which is constant at all depths, B) a 20 km wide vertical board with 5 km gap between Vp and Vs anomalies, which is constant in the direction perpendicular to the profile.
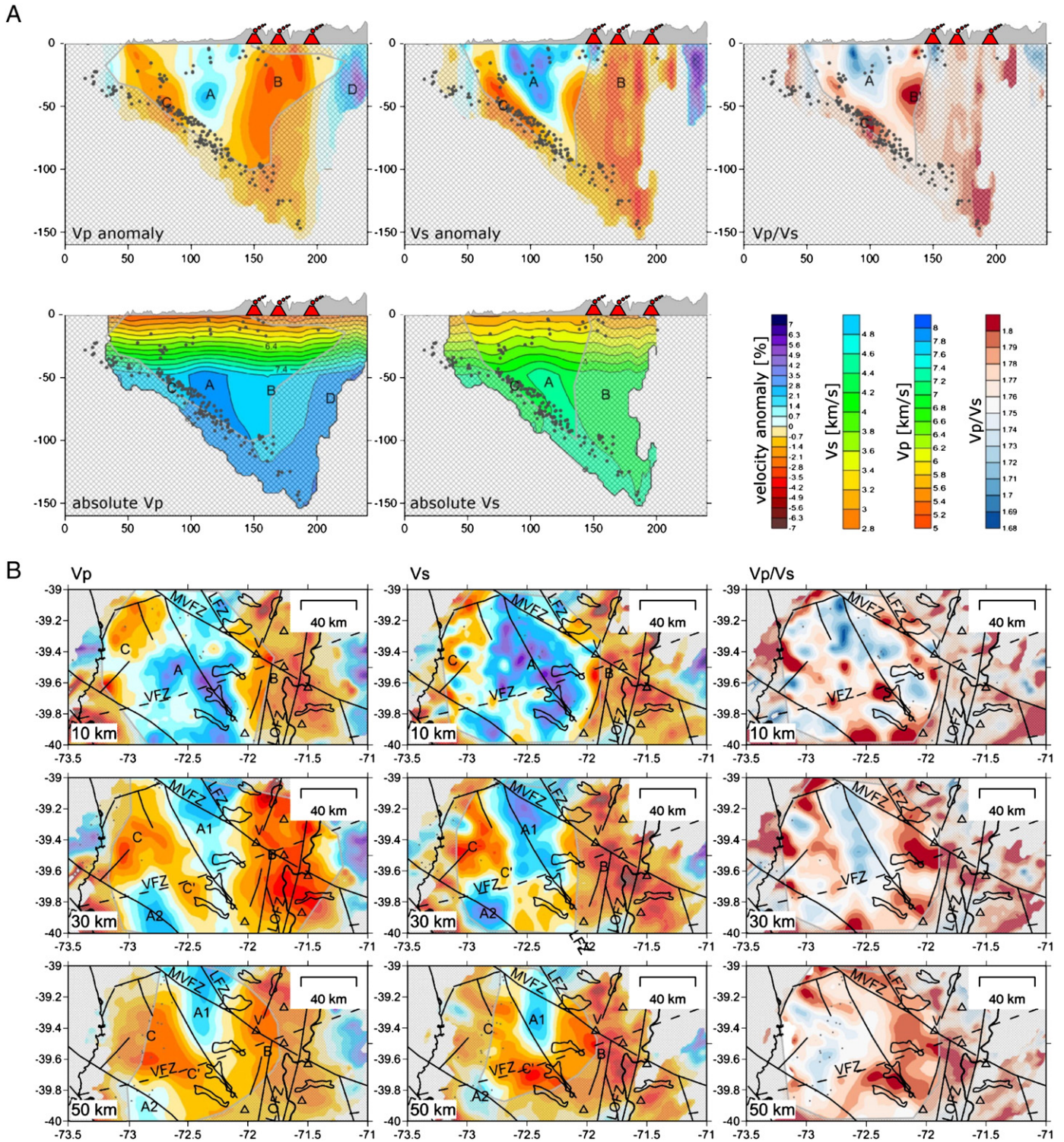
Fig. 5. P- and S-wave velocity anomalies and velocity ratios from tomographic inversion. In addition to the main faults shown in Fig. 2, we display the prolongation of the Valdivia Fracture Zone (dashed line). The location of the Valdivia Fracture Zone is open to some uncertainty, since different positions are given in the literature. We have picked the bathymetric high and prolonged the subducted VFZ along a straight line on top of the slab, which is then projected onto the surface. This position agrees with gravity observations (Wells et al., 2003). Relocalized earthquakes are plotted as grey dots. A) Absolute Vp and Vs velocities, velocity anomalies and Vp/Vs ratios along the profile shown in Fig. 2. The topography and the volcanoes Villarrica, Quetrupillán and Lanin are displayed as reference. B) Vp and Vs anomalies and Vp/Vs ratios at 10, 30, 50 km depth. Values between 1.73 and 1.78 are relatively "normal", only values outside this range are interpreted in the text.

resolution of the obtained model. To investigate the effect of random noise on the result of the tomographic inversion, a bootstrap test (odd/even test) was performed, which consists of performing independent inversions for two different data subsets (here, subsets with odd and even numbers of events). The result of this test (Fig. 6) shows that the main features observed in the tomographic inversion are robustly resolved in both cases. Thus, the random noise in the data does not significantly affect the results.
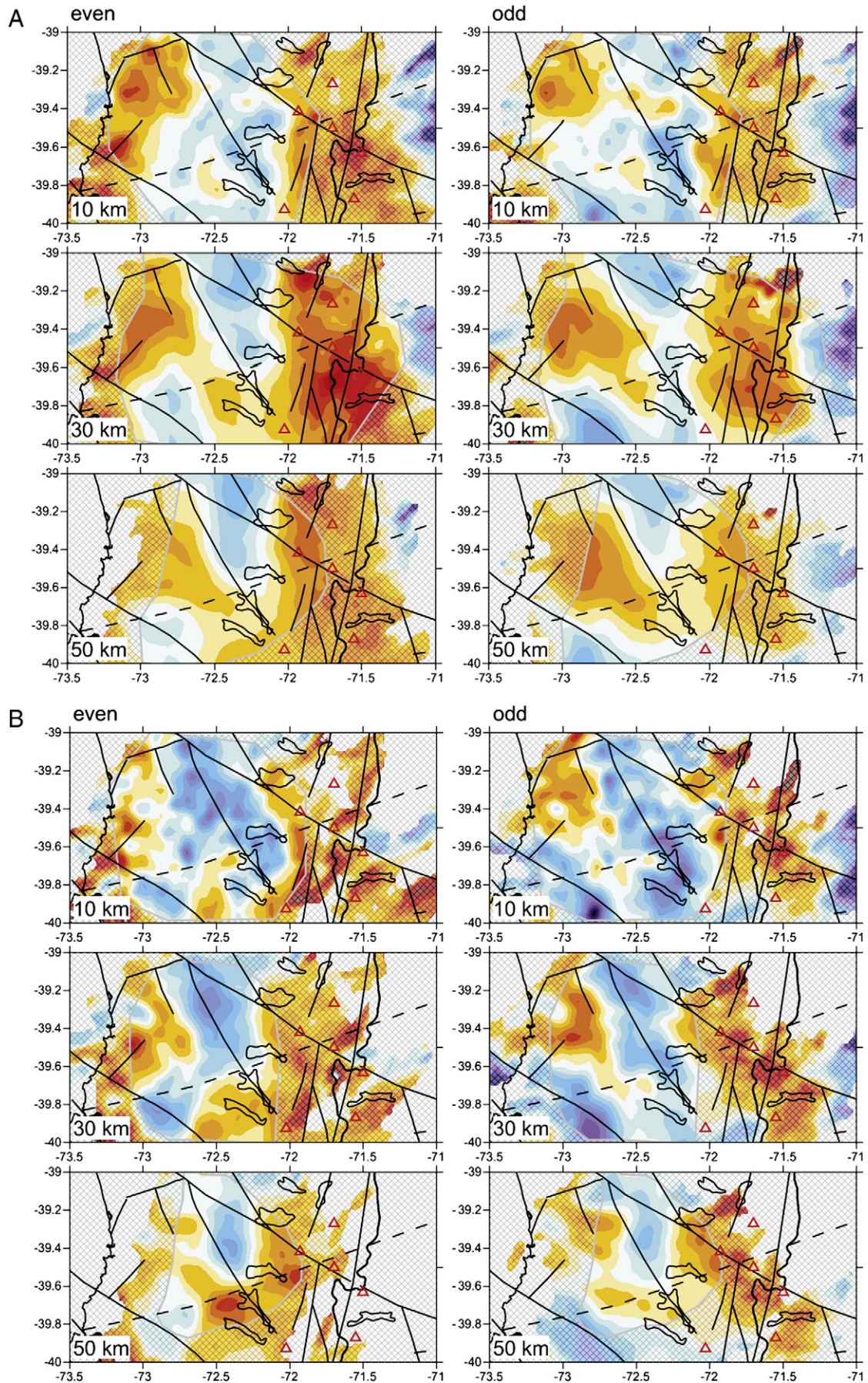
Fig. 6. Bootstrap tests. Tomographic inversion for even vs. odd-numbered data subsets. A) Vp velocities, B) Vs velocities.

We present the 10, 30 and 50 km depth sections for the Vp and Vs anomalies, i.e. deviations from the 1D background velocity model, and one vertical profile normal to the trench (Fig. 5). The deviations from the 1D velocity model are rather small, not exceeding $\pm 5\%$. We first consider the main features in the vertical profile before looking at lateral variations along the trench.

5.1. Vertical profile

In the continental crust, the absolute velocities are layered approximately horizontally, which mainly reflects the velocity gradient of the background model. At a distance of 75–150 km from the trench, a high-velocity anomaly (A) is observed, which in absolute velocities corresponds to fast mantle velocities and upwarping crustal velocity contours. We believe that this part of the velocity model corresponds to the "normal crust and mantle" scenario, with a comparatively fast (Vp = 7.6–7.8 km/s, Vs = 4.4 km/s) mantle underlying the continental crust. This interpretation is supported by the fact that a similar absolute velocity profile (again with a fast mantle and an associated high-velocity anomaly) is again observed beyond the volcanic arc (D, at 200–250 km distance along the profile), although ray coverage in this region is poorer and S-wave velocities could not be reliably recorded here.

Farther from the trench, the mantle velocities are lower down to depths in excess of 100 km, reflected also by a negative velocity anomaly (B) observed in the depth range from the surface to the slab. The large depth extent of this feature is probably caused by the limited vertical resolution; however, it is evident that the velocities in this region are lower than in the adjacent area. This is explained by the presence of fluids and melts beneath the active volcanic arc, which was also observed as a high-conductivity structure in a magnetotellurics study by Brasse and Soyer (2001).

In the coastal area, a second low-velocity anomaly (C) is observed with low mantle velocities. In this region, the low-velocity contours in the mantle dip slightly towards the east. This feature may be associated with a serpentinised mantle wedge or underthrusting of low-velocity fore-arc rocks as proposed by Haberland et al. (2009).

The Vp/Vs velocity ratio supports this general scenario. The "normal" region (A) between the coast and the volcanic arc is characterised by "standard" Vp/Vs ratio around 1.73, whereas those features associated with possible fluid and melt effects (B and C) have considerably higher Vp/Vs up to 1.8 and higher. Down to 70 km, the slab and possible subducting fore-arc material appear as a low-velocity anomaly with somewhat elevated Vp/Vs ratio up to 1.8 (C). Below this depth, Vp/Vs ratio has an average value around 1.76, and the slab does not show particularly low or high velocities. This might indicate that the main dewatering reactions of the upper part of the slab are completed around this depth. However, the resolution of the slab velocities is rather poor, since no events occur below the slab. The low-velocity zone below the volcanic arc is also characterised by increased Vp/Vs ratios, but the strongest increase is more localised in the velocity anomalies (B′) and may be related with fluids moving from the slab towards the volcanic arc. In general, Vp/Vs values above 1.8 cannot be regarded as unique evidence of dehydrating rock because they can be created by mineralogical composition as well (e.g. Christensen, 1996). However, in the present case there is no indication for a compositional change of the subducting rock along the slab whereas it is commonly accepted that the subducting rocks are dehydrated due to the changing pressure–temperature conditions. This second view is supported by the observation that the elevated Vp/Vs ratios are associated with low-velocity anomalies in P and S. Therefore, we favour the interpretation that the velocity anomalies and Vp/Vs ratios probably indicate the presence of fluids although we must keep in mind that compositional differences may provide an alternative interpretation which cannot be ruled out.

5.2. Horizontal anomaly maps

The structures shown in the vertical profile are generally retrieved in the horizontal sections. In particular, we observe the following features:

A) A high-velocity anomaly associated with the crust and fast "normal" mantle in the central region (A). In the north and south adjacent regions, this fast anomaly was associated with the Longitudinal Valley (Bohm et al., 2002; Haberland et al., 2009; Lange et al.), which is disrupted in our study area above the Valdivia Fracture Zone (compare Fig. 1). The tomographic maps at 30 km depth show that the high velocity anomalies look as if they were displaced dextrally by ca. 30 km along the VFZ.

B) A low-velocity anomaly associated with the volcanic arc and LOFZ in the east (B), which is also in agreement with Haberland et al. (2009) and Lange (2008). It is particularly pronounced beneath the Villarrica, Quetrupillán and Lanín Volcanoes, which are aligned along the Mocha-Villarrica Fault Zone. Near the crossing point of the LOFZ with the MVFZ and the extrapolation of the VFZ, we find a distinct maximum of Vp/Vs at lower crustal and upper mantle levels, the projection of which lies next to the three volcanoes. We regard it as an expression of the melt reservoir from which these volcanoes are fed.

C) A low-velocity anomaly close to the coast (C), which we interpret as serpentinised mantle and/or underthrust sedimentary rocks. This structure trends approximately parallel to the trench, but appears to extend further onshore in the central part of the study area (C′), possibly related to the shift in the high velocity anomalies (A1, A2).

While the main features linked with the subduction system are consistent along the trench, a disruption occurs in the tomografic maps for 30 and 50 km depths in the region close to the continuation of the Valdivia Fracture Zone. In particular, the high-velocity feature interpreted as normal mantle wedge appears deformed and interrupted by a low-velocity region. Along the same line, the Vp/Vs velocity ratio is increased to values close to 1.8. We infer from this that the Valdivia Fracture Zone region on the subducting slab may be more hydrated than adjacent regions with normal, not-fractured oceanic crust. This is supported by the observation of a seismicity cluster (Fig. 7) found along the extrapolated trace of the subducting oceanic fracture zone at 80 to 120 km depth (Dzierma et al., submitted for publication). Most of the earthquakes of this cluster show a strike-slip movement suggesting that the Valdivia Fracture Zone is reactivated at depth probably triggered by dehydration. The subducted part of the Valdivia Fracture Zone could represent a major heterogeneity along the subduction zone, interrupting its basic 2D structure by creating the observed low-velocity anomalies where larger amounts of fluids are released in the overriding plate and mantle wedge.

At 30 km depth the central high velocity anomaly ends along the extension of the VFZ. Beyond the VFZ another high velocity anomaly is observed, but displaced by 30 km along the extrapolated fracture zone. There is no doubt that the anomaly pattern as such is not an effect of the inversion (see Synthetic models in the next section). The correlation between the offset of the anomalies and the extrapolation of VFZ suggests that the fracture zone may be the cause of the anomalies.

6. Synthetic models

Several geometries of synthetic models were applied to test the reliability of the inversion. One adequate model is shown in Fig. 8. To reproduce the results, all models needed to include an offset
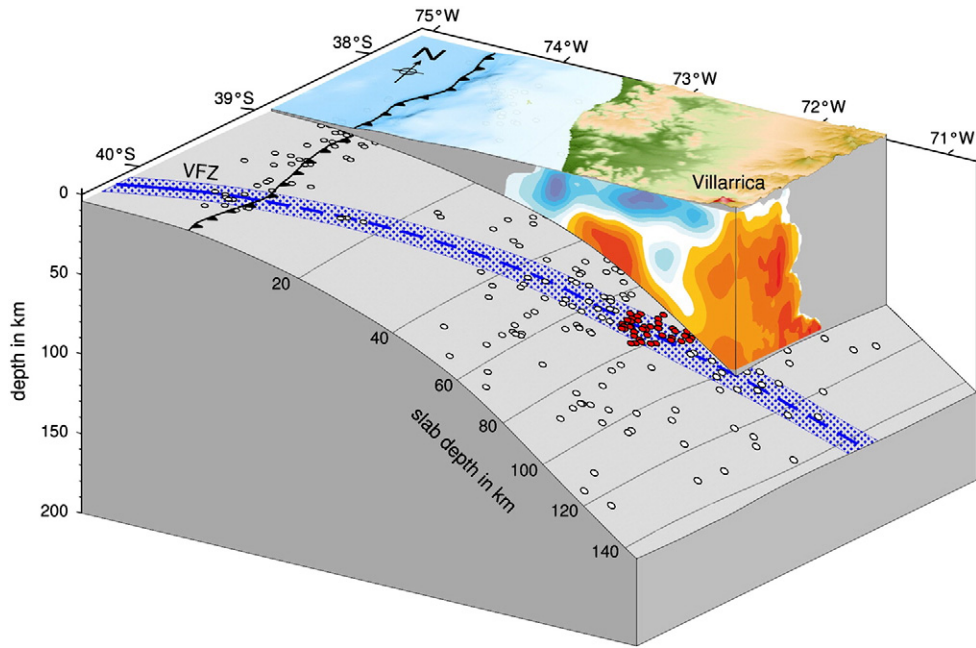
Fig. 7. Seismicity. Concept view of the local seismicity of the study area (presented in detail by Dzierma et al., submitted for publication). The downgoing plate is shown together with the prolongation of the VFZ (blue dashed line). The slab seismicity is projected vertically onto the slab surface (white and red dots). The red events highlight the cluster of seismicity observed close to the main trace of the VFZ. Villarrica volcano in red lies above a tomographic anomaly with reduced velocities.

high-velocity anomaly between ca. 20 and 50 km depth, a slow velocity anomaly near the coast down to at least 30 km depth (but possibly 50 km), and a low-velocity anomaly under the active volcanic arc, which we modelled at 20–50 km. In the upper crust, a fast velocity anomaly in the central region (between the coast and the arc) was also included to better retrieve the shallow structure. A low-velocity zone aligned along the VFZ or a low-velocity region in the mantle wedge above the VFZ both give good results, but are unnecessary for a good model adjustment as long as some broadening in the low-velocity coastal zone is included (as shown Fig. 8).

In general, we found that all input models – whether similar to our preliminary interpretation or not – are well retrieved by the
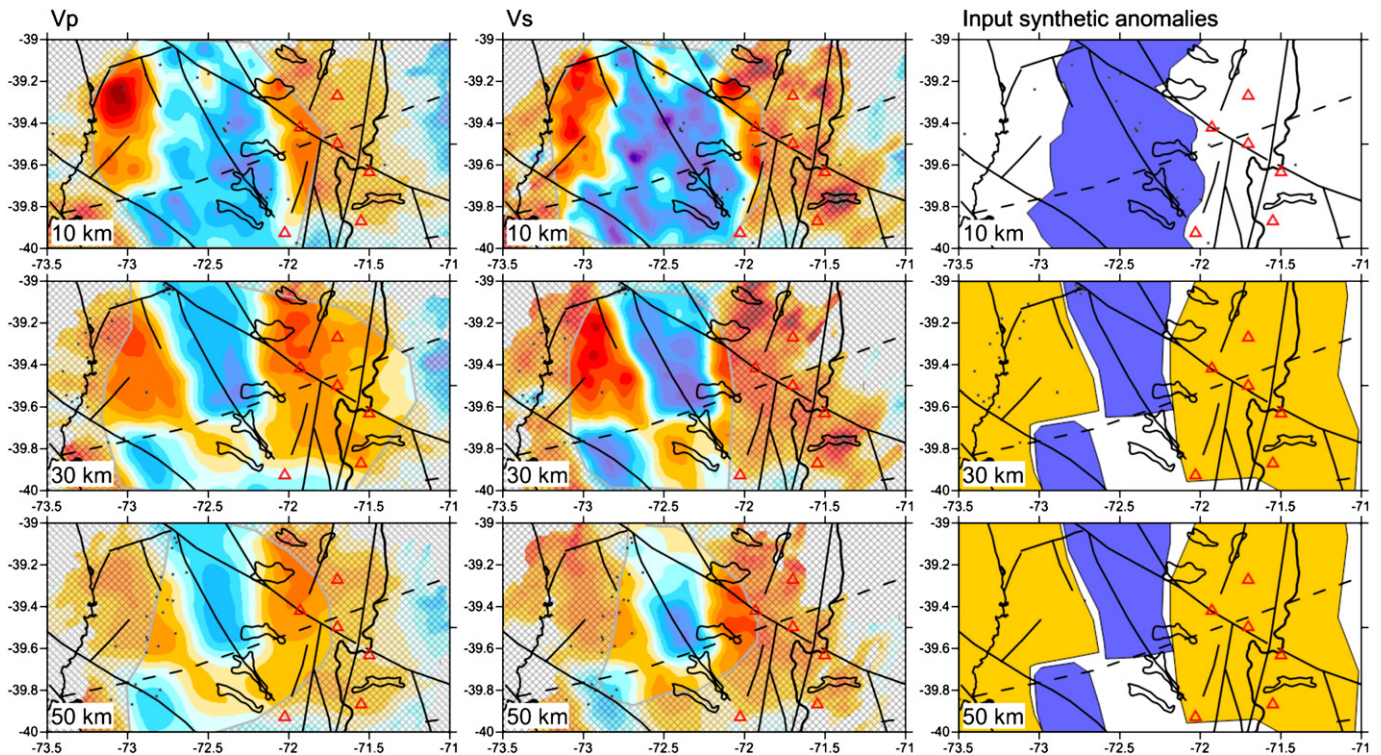

Fig. 8. Synthetic model. The Figure shows our preferred synthetic model with an extended low-velocity wedge close to the VFZ, and two offset high-velocity anomalies in the central region. The colours of the synthetic anomalies are not scaled to match those of the tomographic inversion. The near-surface high velocity anomaly has 5% in Vp and 6% in Vs, reaching down to 15 km depth. All other anomalies are modelled from 20 to 50 km depth. Low-velocity anomalies are modelled with −6% both in Vp and Vs. The interrupted central high-velocity anomaly is assumed to have magnitude 8% Vp and 6% Vs.

inversion. The form of the anomalies within the well-resolved region as determined from ray coverage can be resolved well by the tomography down to depths of 60–70 km, lending credibility to the inversion results. The amplitude of the anomalies is slightly underestimated by a few percent at all depths. To reproduce the observed Vp and Vs anomalies, we need to assume anomalies of the order of 6% in both Vp and Vs.

We tested whether different synthetic models from our preferred interpretation can serve to reproduce the results. In particular, we checked

1. anomalies located in the crust of the overriding plate (Fig. S2),
2. anomalies located in the subducting slab, with an unperturbed upper plate (Fig. S3), and
3. linear anomalies in the upper plate without offset and without an extended area of the low-velocity coastal region (in an attempt to find whether the low-velocity disruption and offset in the high-velocity anomalies might be artificially introduced as an imaging artefact, Fig. S4).

The crust-only recovery test (first test scenario, S2) shows that the crustal anomalies smear into the mantle in the sense that the image occurring at 30 km is repeated at 50 km with 50% and partly more reduced amplitude. The real tomographic slices at 30 and 50 km are indeed somewhat similar, but there are obvious differences, too. First, the strength of the real anomalies does not diminish with depth (as in the case of the crust-only scenario); second, the shape and location of the anomalies and their extrema change (compare, for example, C and C′ at 30 and 50 km). Since the synthetic and real data have the same source-receiver configurations these differences between the S2 scenario and the field tomograms are not likely to be a result of the limited resolution. Therefore, we prefer to consider the change of the anomalies from a depth of 30 to 50 km as evidence that the tomographic patterns cannot be explained by crustal structure alone but require some change in the mantle, too.

Besides the generally low resolution caused by the source-receiver distribution, the anomaly images of the different depth levels grade into each other because of the damping inherent in the tomographic inversion. This circumstance superimposes a certain level of vagueness to any tomographic interpretation, which we tried to assess with the synthetic scenarios in the Appendix (and a number of other geometries not shown here). From these models we infer that

1. The high-velocity anomaly (A) observed in the horizontal sections at 30 and 50 km depth and reaching down to 70 km in the vertical section cannot be explained satisfactorily by crustal structure alone, but points to an involvement of the upper mantle. However, it has to be stated clearly that the exact depth extent cannot be determined from the tomography.
2. The corresponding lithospheric structure has no surface expression,
3. The high velocity anomaly cannot be created only by an offset high-velocity feature in the subducting slab, but *must* involve the overriding plate lower crust and mantle, and
4. The observed abrupt anomaly offset is a real phenomenon not introduced by the imaging process.

The modelling studies hence confirm the existence of low-velocity anomaly close to the coast, which we interpret as a serpentinised mantle wedge and/or underthrust forearc rocks in following the previous work by Bohm (2004), Haberland et al. (2009) and Lange (2008). The low-velocity anomaly extends farther inland in the region close to the subducting Valdivia Fracture Zone, where it interrupts and "shifts" the high-velocity anomalies associated with "normal" fast mantle (and possibly lower crust) velocities. We interpret this as an indication for enhanced fluid release along the trace of the VFZ. The high-velocity anomalies are similar to what is observed

beneath the Central Valley to the north and south of our study area, their interruption and shift may be linked with the absence of a Central Valley in the Villarrica region. Under the volcanic arc, low velocities are observed, which are linked with the presence of melts and fluids under the volcanoes.

7. Discussion

7.1. Strong vs. weak slab interface coupling and the role of the Valdivia Fracture Zone

On the basis of the anomalous gravity signature of this region, and the global observations of a correlation of trench-parallel gravity highs with areas of increase coseismic slip (Wells et al., 2003), Hackney et al. (2006) speculate that the segment between 39 and 40°S is particularly strongly locked in comparison with the adjacent subduction zone segments. The same conclusion is reached by Alasonati Tašárova (2007) based on gravity modelling. Alasonati Tašárova's subsurface model shows an increase of 5 km in slab depth in this segment indicating an increased normal stress on the slab interface. However, neither a receiver function study of this region nor a seismicity study can support the hypothesis of a deepening of the slab (Dzierma et al., submitted for publication; Dzierma et al., in press). In contrast, Moreno et al. (2011) have shown that the accumulated strain after the 1960 earthquake is particularly low in the centre of this same segment of the subduction zone. They propose that the incoming VFZ provides a localised line of weakness in which plate coupling is low due to the larger amount of pore fluids carried by the subducting plate along the fracture zone.

Our tomography results are in good agreement with the interpretation by Moreno et al. (2011). The VFZ fault line marks the southern edge of a forearc region of reduced seismic velocities, together with increased Vp/Vs. This suggests that fluids are present in larger amounts than south of the VFZ, which would explain a local reduction in coupling strength. In this scenario it has to be considered that the VFZ line shown in the figures is basically the prominent southern border of a ca. 50 km wide fault system that can be recognized offshore in the bathymetry of the incoming plate. Therefore, it can be assumed that enhanced fluid release does not only occur along the VFZ fault trace but also in a several 10 km wide swath north of it.

The observed low velocities possibly related to serpentinisation would imply some related reduction in density. It would have to be tested in a future modelling study whether the observed gravity low could be explained by a reduced mantle wedge density as well as with a local increase of the depth of the subducting slab.

The local weakness of plate coupling along the VFZ may explain why the 1960 coseismic slip maxima occurred just to the north and south of the fracture zone, with a reduction of slip in between them just along the line of the VFZ. Possibly, interseismic strain build-up along this line was weaker due to aseismic creep; this would be an analogous situation to the one observed today after the 1960 earthquake. This heterogeneity of preseismic strain build-up could greatly influence the rupture behaviour of future large earthquakes along this part of the margin.

7.2. Geochemical evidence for enhanced fluid release from the slab along the Valdivia Fracture Zone beneath the volcanic front

Geochemical characteristics of volcanic rocks from Llaima and Villarrica Volcanoes compared with the rest of the volcanic front between 35 and 43°S confirms a greater fluid flux from the slab above the subducting VFZ. Ratios of trace elements of different fluid-mobility are typically used in subduction zone volcanic rocks to trace the role of fluids in magma generation (e.g., Elliott et al., 1997; Patino et al., 2000). Fluid-mobile elements, such as U, Ba and Pb, are more strongly enriched than the less mobile elements, such

as Th, Nb and the rare earth elements (REE) in the presence of sub-duction zone fluids. Ratios of more to less fluid mobile elements, such as U/Th, Pb/Ce, and Ba/Th, can be used as proxies of fluid flux from the subducting slab beneath volcanic centres. For relatively fluid immobile elements, ratios of more to less incompatible elements, for example La/Yb and La/Sm, correlate inversely with the degree of melting. Volcanic rock samples from Llaima and Villarrica Volcanoes generally have the highest U/Th, Ba/Nb, Pb/Ce and Pb/Nd and lowest La/Yb of volcanic rocks from the volcanic front between 35 and 43°S (Fig. 9), implying the greatest fluid flux and degrees of melting beneath the volcanic front volcanoes between 39 and 40°S. The addition of slab-derived fluids to the mantle wedge was also observed to peak beneath Villarrica by Morris et al. (1990) and Sigmarsson et al. (2002) based on correlations between U-series disequilibria, $^{226}Ra/^{230}Th$ and $^{238}U/^{230}Th$, with $^{10}Be/^{9}Be$ isotope ratios. These geochemical variations therefore link the high fluid flux to the VFZ. Hydrous fluids/melts serve to lower the solidus temperature in the mantle, which results in greater degrees of melting when the fluid flux is higher. Hence the high fluid flux from the subducting fracture zone system bounded by the VFZ line in the south appears to have caused higher degrees of melting beneath Villarrica and Llaima Volcanoes, providing a possible explanation for why these two volcanoes are among the most active ones in South America.
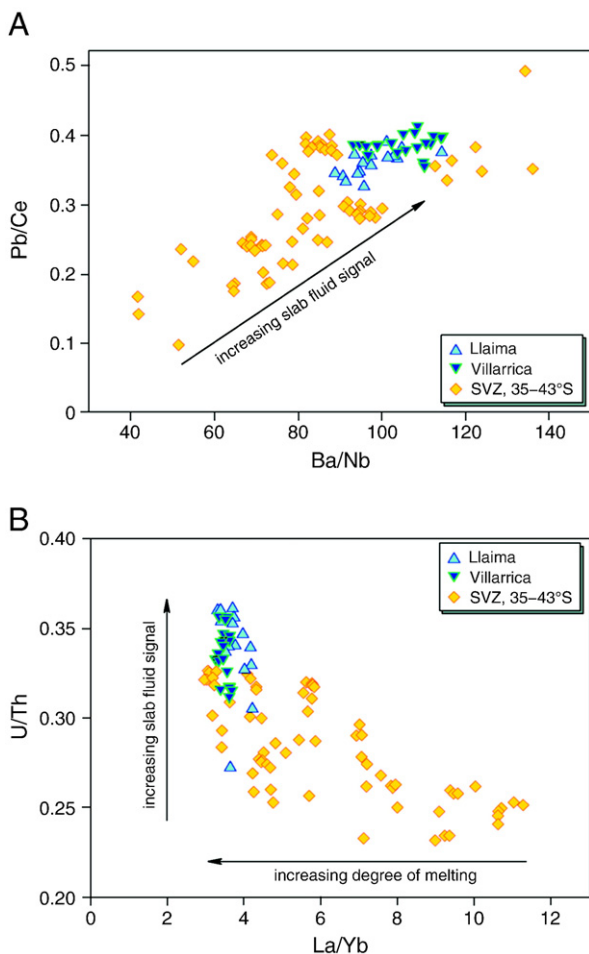

Fig. 9. Geochemical proxies. (A) Pb/Ce versus Ba/Nb and (B) U/Th versus La/Yb of mafic to intermediate volcanic rocks along the Southern Volcanic Zone between 35 and 43°S. Volcanic rocks from Llaima and Villarrica Volcanoes generally show the highest U/Th, Pb/Ce, and Ba/Nb, implying the highest fluid flux beneath these volcanoes. The low La/Yb ratios imply that the highest degrees of melting also took place beneath these volcanoes, as a result of the high fluid fluxes.

7.3. Change of seismic anomalies across the extrapolated VFZ line

The 30 km shift of the Vp and Vs anomaly patterns north and south of the extrapolated VFZ line, visible in the horizontal slices between 30 and 50 km depth, corresponds to the lower continental crust and the upper mantle wedge. It provokes a number of questions:

– Can this anomaly shift be interpreted as the expression of right-lateral displacement along the oceanic subducted Valdivia fracture zone that has coupled into the overriding continental plate? This suggestive idea seems to be supported by the geometrical coinci-dences and by the orientation of the fault movement offshore that would correspond to the displacement of the tomographic anomaly patterns. The following arguments speak against this view: (1) There is no obvious surface expression of a correspond-ing strike slip movement; (2) a decoupling of strike-slip move-ment in the deeper crust from the upper crust, which would solve this problem, does not appear likely because other strike-slip faults, such as the MVFZ, encounter all depth levels of the crust. (3) It is difficult to imagine a coupling mechanism at the plate interface that is strong enough to break the overriding continental plate.
– Can the agreement between the extrapolated VFZ line and the "shift line" of the anomalies be a random coincidence? This possi-bility cannot be ruled out. The basement of our investigation area might be heterogeneously composed comprising, for example, a boundary between two proterozoic terranes such as the Chiloé Block (Moreno et al., 2008), which is supposed to terminate ca. 100 km south of our area. Also, one has to take into account that the deep crust and upper mantle may have been altered by intrusions and metamorphism in a heterogeneous way along the margin.
– Can the N–S change in the anomalies of the overriding plate be explained by N–S changes in the downgoing plate? Across the VFZ the incoming plate changes significantly in age from 26 Myrs in the north to 18 Myrs in the south (at the trench, Tebbens et al., 1997). This age change may be connected with a change in temperature and composition as well. For example, Ruepke et al. (2002) estimated a temperature difference of ca. 100 °C down to 100 km between slabs of similar ages in Central America. Therefore, the phase changes and dehydration of the subducted sediments and oceanic crust and the related hydration of the overriding mantle wedge may take place at shallower depths in the south than in the north of the VFZ. The same argumentation applies also to the VFZ as such. Differences in the depth levels of dehydration and hydration would translate into an apparent horizontal "displacement" of the corresponding to-mographic anomalies because the subducting interface is inclined. The line across which this displacement occurs corresponds to the extrapolated VFZ line. The position of this line as well as the shape of the tomographic anomalies will change with time because the incoming plate subducts obliquely under the continent. This implies that the extrapolated VFZ line and all features connected with it will move to the north over time.

This last scenario appears us to be the most plausible explanation of our observation.

7.4. Termination of the Central Valley

The Central Valley terminates in the north of our investigation area approximately at the Mocha-Villarrica Fault Zone, and starts again south of the extrapolation of the Valdivia Fracture Zone. The movement along the MFVZ and the Lanalhue Fault Zone (LFZ), which splits off the MVFZ near Llaima volcano and runs NW towards Arauco Peninsula, has to be seen in a larger continent scale context.

Both geodetic measurements (Moreno et al., 2008) and geological field evidence (Aragón et al., 2011; Rosenau et al., 2006) indicate that the forearc south of 38°S, the Chiloé Block, is being displaced north along the LOFZ as a consequence of the oblique subduction to the Nazca Plate. This movement is blocked between 38 and 39°S and converted into a complicated transpressional system including block rotation. Based on Aragón et al. (2011) and Rosenau et al. (2006) the termination of the Central Valley can be regarded as a consequence of the compressional components of this movement that counteract subsidence south of the MVFZ. The tomography can confirm this plate kinematic model insofar as there is a change of crustal P- and S-wave velocity structure across a part of the MVFZ, the image of which might tentatively be interpreted as evidence of lateral displacement along the MVFZ. This velocity change is found in the horizontal sections at 10 km depth near the splitting point of MVFZ and LFZ (between 39.3 and 39.4°S and 72 to 72.3°W). The strike of this structure is parallel to the MVFZ and follows this lineament over 30 km. Whether or not the change in lithospheric structure across the extrapolated VFZ (and possibly plate coupling due to enhanced fluid release) has influenced the formation of the complicated deformation pattern in the LOFZ-MVFZ-LFZ-Arauco zone will have to be investigated by modelling in the future.

8. Conclusions

Based on local earthquake tomography, we observe the following main velocity structure along the south-central Chilean subduction zone (39–40°S): a low-velocity anomaly and high Vp/Vs values under the coast indicates a serpentinised mantle wedge and/or underthrust forearc sediments. The central region (which corresponds to the Longitudinal Valley to the north and south of the study area) is underlain by a high-velocity anomaly, interpreted as "normal" fast mantle. Further towards the east, fluid release under the active volcanic arc is expressed by a negative velocity anomaly linked with high Vp/Vs ratios (up to 1.8 and higher). Geochemical proxies confirm a higher fluid flux and degrees of melting beneath the volcanic front in this region, which could lead to greater volcanic activity in this part of the volcanic arc.

Along the trace of the subducting Valdivia Fracture Zone, the coastal low-velocity anomaly extends further into the central region, where it interrupts and shifts the high-velocity anomalies associated with "normal" fast mantle velocities. We interpret this as an indication for enhanced fluid release along the trace of the VFZ, consistent with geochemical results and recent GPS measurements suggesting reduced plate coupling and aseismic slip (Moreno et al., 2011). These results suggest that due to enhanced hydration, the VFZ is indeed a line of weakness in the plate coupling, where less strain accumulates in the interseismic period. The subduction of the VFZ may also provide the ultimate explanation for why Villarrica and Llaima are among the most active volcanoes in South America.

A shift in the high-velocity anomaly underlying the central part may be explained by a N–S change in plate age and hydration across the VFZ. Assuming a temperature increase of the order of 100 °C, dehydration reactions would take place at shallower depth and hence closer to the trench.

The displacement of crustal velocity anomalies along the MVFZ agrees with a plate kinematic model, derived from GPS and geologic observations, that results in a transpressional tectonic regime. This transpressional model is capable to explain the termination of the Central Valley near the MVFZ.

Supplementary materials related to this article can be found online at doi:10.1016/j.epsl.2012.02.006.

References

Alasonati Tašárová, Z., 2007. Towards understanding the lithospheric structure of the southern Chilean subduction zone (36°S–42°S) and its role in the gravity field. Geophys. J. Int. 170, 995–1014 doi:10.111/j.1365-246X.2007.03466.x.

Aragón, E., D'Eramo, F., Castro, A., Pinotti, L., Brunelli, D., Rabbia, O., Rivalenti, G., Varela, R., Spakman, W., Demartis, M., Cavarozzi, C.E., Aguilera, Y.E., Mazzucchelli, M., Ribot, A., 2011. Tectono-magmatic response to major convergence changes in the North Patagonian suprasubduction system; the Paleogene subduction-transcurrent plate margin transition. Tectonophysics 509 (3–4), 218–237. doi:10.1016/j.tecto.2011.06.012.

Barrientos, S.E., 2007. Earthquakes in Chile. In: Moreno, T., Gibbons, W. (Eds.), The Geology of Chile. The Geological Society, London, pp. 263–287.

Barrientos, S.E., Ward, S.N., 1990. The 1960 Chile earthquake: inversion for slip distribution from surface deformation. Geophys. J. Int. 103, 589–598.

Beck, S., Barrientos, S., Kausel, E., Reyes, M., 1998. Source characteristics of historic earthquakes along the central Chile subduction zone. J. South Amer. Earth Sci. 11 (2), 115–129.

Bohm, M., 2004. 3-DLokalbebentomographie der südlichen Anden zwischen 36° und 40°S, PhD Thesis, Freie Universität Berlin, Berlin.

Bohm, M., Lüth, S., Echtler, H., Asch, G., Bataille, K., Bruhn, C., Rietbrock, A., Wigger, P., 2002. The Southern Andes between 36° and 40°S latitude: seismicity and average seismic velocities. Tectonophysics 356, 275–289. doi:10.1016/S0040-195(02)00399-2.

Brasse, H., Soyer, W., 2001. A magnetotelluric study in the southern Chilean Andes. Geophys. Res. Lett. 28 (19), 3757–3760. doi:10.1029/2001GL013224.

Cembrano, J., Lara, L., 2009. The link between volcanism and tectonics in the southern volcanic zone of the Chilean Andes: a review. Tectonophysics 471 (1–2), 96–113. doi:10.1016/j.tecto.2009.02.038.

Cembrano, J., Schermer, E., Laveno, A., Sanhueza, A., 2000. Contrasting nature of deformation along an intra-arc shear zone, the Liquiñe-Ofqui fault zone, southern Chilean Andes. Tectonophysics 319 (2), 129–149. doi:10.1016/S0040-1951(99)00321-2.

Charrier, R., Pinto, L., Rodríguez, M.P., 2007. Tectonostratigraphic evolution of the Andean Orogen in Chile. In: Moreno, T., Gibbons, W. (Eds.), The Geology of Chile. The Geological Society, London, pp. 21–114.

Christensen, N.I., 1996. Poisson's ratio and crustal seismology. J. Geophys. Res. 101 (B2), 3139–3156. doi:10.1029/95JB03446.

Comte, D., Eisenberg, A., Lorca, E., Pardo, M., Ponce, L., Saragoni, R., Singh, S.K., Suárez, G., 1986. The 1986 Central Chile Earthquake: a repeat of previous Great Earthquakes in the region? Science 233 (4762), 449–453. doi:10.1126/science.233.4762.449 1986.

Delouis, B., Nocquet, J.-M., Vallée, M., 2010. Slip distribution of the February 27, 2010 Mw = 8.8 Maule Earthquake, central Chile, from static and high-rate GPS, InSAR, and broadband teleseismic data. GRL 37 (L17305), 7 doi: 10.1029/2010gl043899.

DeMets, C., Gordon, R.G., Argus, D.F., 2010. Geologically current plate motions. Geophys. J. Int. 181 (1), 1–80. doi:10.1111/j.1365-246X.2009.04491.x.

Dzierma, Y., Wehrmann, H., 2010. Statistical eruption forecast for the Chilean Southern Volcanic Zone: typical probabilities of volcanic eruptions as baseline for possibly enhanced activity following the large 2010 Concepción earthquake. Nat. Hazards Earth Syst. Sci. 20, 2093–2108. doi:10.5194/nhess-10-2093-2010.

Dzierma, Y., Thorwart, M., Rabbel, W., in press. Moho topography and subducting oceanic slab of the Chilean continental margin in the maximum slip segment of the 1960 Mw 9.5 Valdivia (Chile) earthquake from P-receiver functions, Tectonophysics.

Dzierma, Y., Thorwart, M., Rabbel, W., Siegmund, C., Comte, D., Bataille, K., Iglesia, P., Prezzi, C., submitted for publication. Seismicity near the slip maximum of the 1960 Mw 9.5 Valdivia earthquake (Chile): Plate interface lock and active faults within the crust and subducted slab, JGR (Solid Earth).

Elliott, T., Plank, T., Zindler, A., White, W., Bourdon, B., 1997. Element transport from slab to volcanic front at the Mariana arc. J. Geophys. Res. 102 (B7), 14,991–15,019. doi:10.1029/97JB00788.

Haberland, C., Rietbrock, A., Lange, D., Bataille, K., Dahm, T., 2009. Structure of the seismogenic zone of the southcentral Chilean margin revealed by local earthquake traveltime tomography. JGR 114 (B01317), 17. doi:10.1029/2008JB005902.

Hackney, R., Echtler, H.P., Franz, G., Götze, H.-J., Lucassen, F., Marchenko, D., Melnick, D., Meyer, U., Schmidt, S., Tašárová, Z., Tassara, A., Wienecke, S., 2006. The segmented overriding plate and coupling at the south-central Chilean margin (36–42°S). In: Oncken, O., Chong, G., Franz, G., Giese, P., Götze, H.-J., Ramos, V.A., Strecker, M.R., Wigger, P. (Eds.), The Andes — Active Subduction Orogeny. Springer, Berlin, Heidelberg, pp. 355–374. doi:10.1007/978-3-540-48684-8_17.

Hyndman, R.D., Yamano, M., Oleskevich, D.A., 1997. The seismogenic zone of subduction thrust faults. The Island Arc 6, 244–260.

Koulakov, I., 2009. LOTOS code for local earthquake tomographic inversion: benchmarks for testing tomographic algorithms. Bull. Seis. Soc. Am. 99 (1), 194–214. doi:10.1785/0120080013.

Lange, D., 2008. The South Chilean Subduction Zone between 41° and 43.5°S: Seismicity, structure and state of stress, PhD Thesis, Universität Potsdam, Potsdam.

Lomnitz, C., 2004. Major earthquakes in Chile: a historical survey, 1535–1960. Seismol. Res. Lett. 75 (3), 368–378. doi:10.1785/gssrl.75.3.368.

Melnick, D., Echtler, H.P., 2006. Morphotectonic and geologic digital map compilations of the south-central Andes (36°–42°S). In: Oncken, O., Chong, G., Franz, G., Giese, P., Götze, H.-J., Ramos, V.A., Strecker, M.R., Wigger, P. (Eds.), The Andes — Active Subduction Orogeny. Springer, Berlin, Heidelberg, pp. 565–568.

Moernaut, J., De Batist, M., Charlet, F., Heirman, K., Chapron, E., Pino, M., Brümmer, R., Urrutia, R., 2007. Giant earthquakes in South-Central Chile revealed by Holocene mass-wasting events in Lake Puyehue. Sediment. Geol. 195, 239–256. doi:10.1016/j.sedgeo.2006.08.005.

Moreno, M.S., Klotz, J., Melnick, D., Echtler, H., Bataille, K., 2008. Active faulting and heterogeneous deformation across a megathrust segment boundary from GPS data, south central Chile (36–39°S). Geochem. Geophys. Geosyst 9, Q12024. doi:10.1029/2008GC002198.

Moreno, M.S., Bolte, J., Klotz, J., Melnick, D., 2009. Impact of megathrust geometry on inversion of coseismic slip from geodetic data: application to the 1960 Chile earthquake. Geophys. Res. Lett. 36, L16310. doi:10.1029/2009GL039276.

Moreno, M., Rosenau, M., Oncken, O., 2010. 2010 Maule earthquake slip correlates with pre-seismic locking of Andean subduction zone. Nature 467, 198–202. doi:10.1038/nature09329.

Moreno, M., Melnick, D., Rosenau, M., Bolte, J., Klotz, J., Echtler, H., Baez, J., Bataille, K., Chen, J., Bevis, M., Hase, H., Oncken, O., 2011. Heterogeneous plate locking in the South-Central Chile subduction zone: Building up the next great earthquake. Earth Planet. Sci. Lett. 305 (3–4), 413–414 doi:10.1016/j.epsl.2011.03.025.

Morris, J., Leeman, W.P., Tera, F., 1990. The subducted component in island arc lavas: constraints from Be isotopes and B–Be systematics. Nature 344, 31–36.

Patino, L.C., Carr, M.J., Feigenson, M.D., 2000. Local and regional variations in Central American arc lavas controlled by variations in subducted sediment input. Contrib. Mineral. Petrol. 138, 265–283.

Ranero, C., Grevemeyer, I., Sahling, H., Barckhausen, U., Hensen, C., Wallmann, K., Weinrebe, W., Vannucchi, P., von Huene, R., McIntosh, K., 2008. Hydrogeological system of erosional convergent margins and its influence on tectonics and interplate seismogenesis. Geochem. Geophys. Geosyst. 9 (Q03S04), 17. doi:10.1029/2007GC001679.

Rehak, K., Strecker, M.R., Echtler, H.P., 2008. Morphotectonic segmentation of an active forearc, 37°–41°S, Chile. Geomorphology 94 (1–2), 98–116. doi:10.1016/j.geomorph.2007.05.002.

Robinson, D.P., Das, S., Watts, A.B., 2006. Earthquake rupture stalled by a subducting fracture zone. Science 312, 1203. doi:10.1126/science.1125771.

Rosenau, M., Melnick, D., Echtler, H., 2006. Kinematic constraints on intra-arc shear and strain partitioning in the southern Andes between 38°S and 42°S latitude. Tectonics 25, TC4013. doi:10.1029/2005TC001943.

Ruepke, L.H., Phipps Morgan, J., Hort, M., Connolly, J.A.D., 2002. Are the regional variations in Central American arc lavas due to differing basaltic versus peridotitic slab sources of fluids? Geology 30, 1035–1038. doi:10.1130/0091-7613(2002)030<1035:ATRVIC>2.0.CO;2.

Sigmarsson, O., Chmeleff, J., Morris, J., López-Escobar, L., 2002. Origin of ^{226}Ra–^{230}Th disequilibria in arc lavas from southern Chile and implications for magma transfer time. Earth Planet. Sci. Lett. 196, 189–196.

Sparkes, R., Tilmann, F., Hovius, N., Hillier, J., 2010. Subducted seafloor relief stops rupture in South American great earthquakes: Implications for rupture behaviour in the 2010 Maule, Chile earthquake. Earth Planet. Sci. Lett. 298, 89–94. doi:10.1016/j.epsl.2010.07.029.

Stern, C.R., 2004. Active Andean volcanism: its geologic and tectonic setting. Rev. Geol. Chile 31–2, 161–206.

Tebbens, S.F., Cande, S.C., Kovacs, L., Parra, J.C., LaBrecque, J.L., Vergara, H., 1997. The Chile ridge: a tectonic framework. J. Geophys. Res. 102 (B6), 12,035–12,059.

Wells, R.E., Blakely, R.J., Sugiyama, Y., Scholl, D.W., Dintermann, P.A., 2003. Basin-centered asperities in great subduction zone earthquakes: a link between slip, subsidence, and subduction erosion? J. Geophys. Res. 108 (B10), 2507. doi:10,1029/2002JB002072.